

A Chandra study of X-ray sources in the field of the $z=2.16$ radio galaxy MRC 1138-262

L. Pentericci¹, J.D. Kurk², C.L. Carilli³, D.E. Harris⁴, G.K. Miley², and H.J.A. Röttgering²

¹ Max-Planck-Institut für Astronomie, Königstuhl 17, D-69117, Heidelberg, Germany

² Sterrewacht Leiden, P.O. Box 9513, 2300 RA, Leiden, The Netherlands

³ National Radio Astronomy Observatory, P.O. Box 0, Socorro NM, 87801, USA

⁴ Smithsonian Astronomical Observatory, Harvard-Smithsonian Center for Astrophysics, 60 Garden Street, Cambridge, MA 02138

Received date / Accepted date

Abstract.

We present results from a *Chandra X-ray Observatory* study of the field X-ray source population in the vicinity of the radio galaxy MRC 1138-262. Many serendipitous X-ray sources are detected in an area of $8' \times 8'$ around the radio source and 90% are identified in our deep VLT images. The space density of such sources is higher than expected on the basis of the statistics of *ROSAT* and *Chandra* deep surveys. The most likely explanation is in terms of a concentration of AGN associated with the protocluster at $z = 2.16$ which was found around the radio galaxy in previous studies. Two sources have a confirmed spectroscopic redshift close to that of the radio galaxy, and for three more sources other observations suggest that they are associated with the protocluster. Four of these five X-ray sources form, together with the radio galaxy, a filament in the plane of the sky. The direction of the filament is similar to that of the radio source axis, the large scale distribution of the other protocluster members, the 150 kpc-sized emission-line halo and the extended X-ray emission associated with the radio galaxy.

The majority of optically identified X-ray sources in this field have properties consistent with type I AGN, a few could be soft, low luminosity galaxies, one is probably an obscured (type II) AGN and one is a star. These statistics are consistent with the results of deep X-ray surveys.

Key words. Galaxies: active – Galaxies: clusters: general – X-rays: galaxies: clusters – X-rays: general

1. Introduction

Since its launch, the *Chandra X-ray Observatory* has been providing the deepest and sharpest images of the X-ray sky ever: one of its most remarkable characteristics is its high spatial resolution ($< 1''$) and astrometric precision ($\sim 1''$), well matched to typical optical and near infrared (NIR) imaging resolutions. This allows unambiguous identifications of faint X-ray sources and the possibility to study the morphologies of the X-ray emitting host galaxies.

We have recently observed the radio galaxy MRC 1138-262, and the surrounding field, with *Chandra* to study the extended X-ray emission associated with this radio source (Carilli et al. 2002), which was previously detected with *ROSAT*. This radio galaxy at redshift 2.16 has a quite complex optical and NIR morphology, resembling a massive galaxy in the early stages of formation and it is embedded in a giant Ly α halo (Pentericci et al. 1997). Deep VLT observations have shown that MRC 1138-262

resides at the center of a protocluster consisting of at least 20 confirmed cluster members (Pentericci et al. 2000, Kurk et al. 2002b).

Chandra's great sensitivity allows the detection of many X-ray emitters in the field besides the main target, even in observations with modest exposure times (a few ten thousand seconds in our case). In this paper we report on these serendipitous X-ray sources: we find an excess of soft X-ray sources in the field, as compared to the predictions for a non-cluster field based on the $\log N - \log S$ relation derived from deep *ROSAT* and *Chandra* measurements. We present optical identifications of the X-ray sources, discuss their nature and their possible relation to the protocluster structure at redshift 2.16.

Throughout the paper we assume a flat, Λ -dominated universe with $H_0 = 65 \text{ km s}^{-1} \text{ Mpc}^{-1}$, $\Omega_M = 0.3$ and $\Omega_\Lambda = 0.7$.

2. X-ray observations

2.1. Source detection

The field of the radio galaxy MRC 1138-262 was observed for 39.5 ksec on June 6, 2000, with the back-illuminated ACIS-S CCD detector on the *Chandra X-ray Observatory*. Standard ACIS settings were used: TE mode with 3.2 s readout and 'faint' telemetry format. The principal aim of this observation was to study the morphology of the extended X-ray emission associated with the central radio galaxy. We refer to Carilli et al. (2002) for a detailed description of the observations, data processing and results on the main target.

The radio galaxy was positioned $\sim 1.5'$ from the standard aim point on the ACIS-S3 chip. Besides MRC 1138-262, many fainter X-ray emitters are registered on this chip. To localize these serendipitous sources we applied the WAVDETECT algorithm (Freeman et al. 2002) of the Chandra Interactive Analysis of Observations (CIAO) software. Given the sensitivity of the observation, we expect to detect mostly sources with soft X-ray spectra. For this reason and to improve the S/N (the background is lower at lower energies), we have limited the energy range for source detection to a maximum of 2 keV. We detect a total of 21 sources on the S3 chip, including the nucleus of the radio galaxy (but excluding the extended emission around this source), of which 18 have $S/N > 3$. All sources are clearly visible by eye. As a check of the validity of the detections, we have also applied the CELLDTECT algorithm of CIAO with a S/N limit of 2.5. This algorithm recovers most of the sources, with the exception of the faintest. Further confirmation of the reality of the X-ray sources comes from the fact that they all have an optical identification.

2.2. Photometry and astrometry

For each detected source with $S/N > 3$ in the soft band we report in Table 1: the source coordinates, the aim point distance in arcminutes, the net photon count for the 0.5–2 keV (soft band S) and the 2–10 keV (hard band H) energy ranges, the corresponding flux, the aperture in arcsec 2 , and the hardness ratio $(H-S)/(H+S)$.

The photometry was performed through elliptical apertures, with properties (i.e. sigma and PA) given by the region file produced by WAVDETECT¹. The minimum size of the apertures is $\sim 1''.6$, implying that at energies below 6 keV, which includes the majority of the detected photons, more than 80% of the energy of the X-ray sources is included (see Fig. 4.15 in Dobrzycki et al. 2001).

¹ These apertures are not the same as the WAVDETECT source cells, which have arbitrary shapes. However the photometry output of WAVDETECT through these cells in the soft band agrees very well with the manual photometry through the elliptical apertures. This indicates that, because our sources are almost all quite compact, the shape of WAVDETECT apertures can be well approximated by ellipses.

The counts reported in Table 1 are background subtracted and corrected for vignetting. The background counts are negligible for most sources. We estimate the background in the soft and hard band to increase the counts by 0.01 and 0.04 per pixel, respectively. In the soft band this amounts to one background count for a 100 pixel aperture, implying that for all detected sources (except #1), the number of background counts expected are less than one. In the hard band the background counts are not negligible for the largest sources. The vignetting correction was done for the sources located $> 2'$ from the aim point of the telescope. Fig. 4.4 of the *Chandra* Proposer's Observatory Guide shows that the telescope effective area decreases almost linearly with off-axis angle, averaged over azimuth. Following Cappi et al. (2001), we approximate the curves of effective area for photon energies of 1.5 keV and 4.5 keV with linear functions and use these to correct the soft and hard band counts, respectively. Note that the corrections are $< 4\%$ for all sources except for #1.

The net count rates were converted into fluxes assuming a power law spectrum with a Galactic absorption column along the line of sight of $N_H = 4.5 \times 10^{20} \text{ cm}^{-2}$ (Stark et al. 1992) and a standard photon index of $\Gamma = 2.0$ for the soft band and $\Gamma = 1.7$ for the hard band. These spectral models were chosen to allow a comparison with other observations such as the *ROSAT* and *Chandra* Deep Fields. The total fluxes are only weakly dependent on the spectral slopes and Galactic column density assumed.

Astrometric positions were initially determined from the ACIS-S aspect solution. After the identification of the X-ray sources with objects on a deep, ground-based *I* band image discussed in Sect. 3, we refined the relative astrometry between the X-ray frame and the optical image. We used the optical and X-ray positions of the 6 sources which are unresolved in both images and not saturated on the *I* band: these include the nucleus of MRC 1138-262 and two more sources with secure redshift identifications (see below). Subsequently, we registered the images using a general geometric transformation, resulting in a relative astrometric accuracy of approximately $0''.1$. The results are consistent with the shift of $0''.5 \pm 0''.1$ in right ascension and $-0''.2 \pm 0''.1$ in declination that Carilli et al. (2002) applied to the image based on the position of the nucleus of 1138-262 alone (e.g. for source #7 which is the radio galaxy nucleus, the shifts are $0''.45$ and $-0''.14$ respectively). The absolute astrometry of the *I* band image was calibrated using 18 stars of the USNO catalog (Monet et al. 1998) resulting in an accuracy better than $0''.2$.

3. Optical identification of serendipitous X-ray sources

Deep multicolour optical and near infrared images of the field were obtained with the VLT FORS and ISAAC instruments during 2000 and 2001. Details of the observations are reported in Kurk et al. (2002a). To identify the X-ray sources we have used the *I* band image, which is the deepest available having a limiting magnitude of 26.5

Table 1. X-ray point sources in the field of MRC 1138-262

N (1)	RA (2)	Dec (3)	θ (4)	Soft cnts (5)	Soft flux (6)	Hard cnts (7)	Hard flux (8)	Aperture (9)	HR (10)
1	11:40:36.44	-26:24:09.9	6.7	56.4 \pm 7.2	5.0			340	<-0.9
2	11:40:38.84	-26:29:10.3	3.6	9.2 \pm 3	0.8			2.2	<-0.5
3	11:40:39.70	-26:28:45.0	3.5	42.9 \pm 6.5	3.8			6.0	-0.8
4	11:40:44.21	-26:31:29.8	3.2	11.2 \pm 3.3	1.0	9.3 \pm 3	5.4	2.0	-0.1
5	11:40:44.47	-26:29:20.7	2.4	12 \pm 3.4	1.1			4.6	-0.4
6	11:40:45.96	-26:29:16.7	2.0	70 \pm 8.4	6.2	11 \pm 3.3	6.4	6.0	-0.7
7	11:40:48.34	-26:29:08.7	1.5	460 \pm 21.5	40.5	192 \pm 14	111.7	7.5	-0.4
8	11:40:49.55	-26:25:41.5	3.9	50.4 \pm 7	4.4			51.6	-0.8
9	11:40:52.84	-26:29:11.2	0.6	58 \pm 7.6	5.1	9 \pm 3	5.2	6.0	-0.7
10	11:40:54.21	-26:29:43.5	0.4	24 \pm 5	2.1			7.5	-0.7
11	11:40:54.66	-26:29:28.1	0.2	67 \pm 8.2	5.9			5.3	-0.9
12	11:40:58.17	-26:30:27.1	1.2	15 \pm 3.9	1.3			4.4	-0.3
13	11:40:59.24	-26:32:03.2	2.8	31.2 \pm 5.6	2.6	19.0 \pm 4.3	10.0	26.4	-0.2
14	11:40:59.45	-26:31:56.2	2.7	129.5 \pm 11.3	11.3	28.5 \pm 5.3	16.5	31.0	-0.6
15	11:40:59.70	-26:32:07.5	2.5	11 \pm 3.3	1.0			9.2	<0.6
16	11:41:02.43	-26:27:45.0	2.3	19.5 \pm 4.4	1.7	13.0 \pm 3.6	7.6	85.0	-0.2
17	11:41:03.00	-26:27:34.2	2.5	22.6 \pm 4.8	2.0			107	<-0.8
18	11:41:03.93	-26:30:48.5	2.4	64 \pm 8	5.6	126 \pm 11.2	73.3	24.5	+0.3

Notes: (1) Number in X-ray point source catalog (2&3) Right Ascension and declination in J2000 coordinates (4) Distance in arcminutes from aim point of telescope (5) Net photon counts in the soft band (0.5–2 keV) (6) X-ray flux in 10^{-15} erg cm $^{-2}$ s $^{-1}$ in the soft band assuming a power law spectrum with photon index $\Gamma = 2.0$ (7) Net photon counts in the hard band (2–10 keV) (8) X-ray flux in 10^{-15} erg cm $^{-2}$ s $^{-1}$ in the hard band assuming a power law spectrum with photon index $\Gamma = 1.8$ (9) Aperture in arcsec 2 used for the photometry (10) Hardness ratio (H–S)/(H+S)

(except at the edges of the field) and was obtained with a seeing of 0.65''. The total field of view of the dithered FORS image is 0.016 deg 2 and its intersection with the ACIS S3 chip is 0.0154 deg 2 ; the NIR information is only available for the central part of the field.

One of the X-ray point sources (#1) lies outside the region covered by our FORS image, amongst others due to a difference in the orientation of the observations. All other sources are identified in the I band image, with the exception of two that lie in the arms of a nearby spiral galaxy. The coordinates of all optical counterparts deviate less than $\sim 1''.2$ from the X-ray coordinates and most of the sources are coincident within the astrometric uncertainty. Given the depth of our I band observations, the probability that one of the X-ray sources coincides with an optical source not associated with the X-ray source is non-negligible, about 9%, even using a small error circle of 1''.2 radius, corresponding to the largest separation between the X-ray sources and their optical identifications. This means that one (1.35) of the 15 identifications could be spurious. However, all but one of the optical counterparts are substantially brighter (2–3 magnitudes) than the detection limit of the VLT image. At these magnitudes, the probability that an X-ray source coincides with an unassociated optical object is much smaller and their identification is thus more secure.

The optical identifications are listed in Table 2, where we report the difference in position between the X-ray source center and the optical counterpart center (as determined by SExtractor, Bertin & Arnouts 1996), the to-

tal I band magnitude, the I band stellaricity index from SExtractor, which indicates the extendedness of the object (1.0 is unresolved, 0.0 is extended), the redshift if available or an estimate of the redshift, the implied X-ray luminosity, and the soft X-ray to visual band flux ratio computed using R band magnitudes. We cross-correlated the X-ray sources with our catalog of objects with excess emission in narrow band filters corresponding to H α and/or Ly α at $z \sim 2.16$, i.e. the redshift of the radio galaxy (Kurk et al. 2000) and we report any such identification in Table 2. We have also checked our deep 1.4 GHz VLA radio images of this field (unpublished) to search for possible radio counterparts: besides the central radio galaxy we detect weak unresolved emission only from the nucleus of the spiral galaxy (object #14).

Here we briefly discuss some characteristics of individual sources.

Source #3 is identified with a faint QSO (Ly α emitter #1687 in Pentericci et al. 2000) at $z \sim 2.185 \pm 0.005$ (where the uncertainty is mainly due to the presence of absorption features), showing broad Ly α , Si IV and C IV emission lines in its optical spectrum.

Source #5 is identified with a faint extended object, having a color $R - K = 5.8$ ($I - K = 5.3$) such that it can be classified as an Extremely Red Object (ERO, Elston et al. 1988). A spectrum of this object has not yet been obtained, but its colors indicate that it could be a galaxy containing an evolved stellar population at $z > 1.5$ or a dust reddened starburst galaxy at $z \sim 2$ (see the discussion in Kurk et al. 2002a).

Table 2. Optical identifications of X-ray sources

N (1)	Δ RA (2)	Δ Dec (3)	m_I (4)	$B - I$ (5)	S (6)	Redshift (7)	L_x (8)	$\log(\frac{S_x}{S_{opt}})$ (9)	ID (10)		
1			Outside I-band image								
2	-0.12	-0.07	18.6	5.2	0.99			-1.3			
3	0.12	-0.06	22.9	1.4	0.98	2.185	1.5	0.5	AGN, Ly α emitter		
4	-0.70	0.23	23.1	3.9	0.02			0.5			
5	0.09	0.01	25.3	1.6	0.52	~ 2	0.43	0.7	ERO ($I - K > 5.3$)		
6	0.01	-0.07	20.8	1.8	0.98	2.157	2.5	-0.2	AGN, H α emitter		
7	0.00	0.06	22.0	1.3	0.05	2.156	16.3	1.2	Radio galaxy		
8	0.88	0.10	16.6	3.4	1.00	0		-2.4	star?		
9	-0.10	0.04	21.7	1.6	0.98	~ 2.16	2.1	0.0	Ly α emitter		
10	0.10	-0.03	17.8	2.7	0.03			-1.8	spiral galaxy		
11	-0.03	-0.0	17.1	4.4	0.99			-1.4			
12	-0.34	-0.11	20.3	2.8	0.03			-0.9	elliptical		
13			in spiral ^a								
14	-1.03 ^b	-0.07 ^b	15.9	2.5	0.02			-1.5	IRAS/spiral gal.		
15			in spiral ^a								
16	0.51	-0.19	22.9	1.7	0.19	~ 2.16	0.67	0.1	Ly α emitter		
17	0.58	1.03	18.5	4.9	0.99			-1.1			
18	-0.74	0.02	21.1	2.9	0.16			-0.1	merger ^c		

Notes: (1) Number in X-ray point source catalog (2&3) Distance between X-ray source and optical identification in RA and Dec (both in arcseconds) (4) I band magnitude (5) $B - I$ colour (6) I band stellaricity index from SExtractor: from 0.00 (extended source) to 1.00 (point source) (7) Redshift (either secure or an estimate) (8) X-ray luminosity in 10^{44} erg s $^{-1}$ (9) Logarithm of the X-ray to optical flux ratio (10) Optical identification

^a There are three sources inside the optical extent of one nearby spiral galaxy; #14 coincides with the nucleus

^b The nucleus of this bright spiral is saturated on the optical image, so the optical position is known only with some uncertainty

^c Merger or interacting system with tidal arms

Source #6 is identified with another faint quasar at $z = 2.157 \pm 0.002$ showing very broad H α emission in the near infrared spectrum (Kurk et al. 2002b).

Source #7 is the nucleus of the radio galaxy MRC 1138-262 at $z = 2.156$ and is extensively discussed in Carilli et al. (2002).

Source #9 is identified with a faint point source which also has excess Ly α emission in the narrow band images corresponding to redshift ~ 2.16 . No spectrum has been obtained yet.

Source #14 coincides with the nucleus of a spiral galaxy, most probably identified with IRAS F11384-2615 which has been detected by IRAS at both 60 and 100 μ m (Moshir et al. 1990).

Source #16 is a candidate Ly α emitter with very strong and extended Ly α emission. It is very likely another AGN at $z = 2.16$ encompassed by a Ly α halo (Kurk et al. 2002a). Because this object is at the very edge of the I band image, it was not included in the original sample of candidate Ly α emitters (Kurk et al. 2000) and an optical spectrum was not obtained.

Of the other sources, #10 is associated with the nucleus of a spiral galaxy; #13 and #15 lie in the arms of the spiral galaxy #14 and cannot be identified in the optical bands. Four sources (#2, #8, #11 and #17) are identified with unresolved objects with I band magnitudes in the range 16.6–18.6. The brightest of these might be a

star as suggested by the X-ray to optical spectral index (see below). Source #12 coincides with a 20th magnitude elliptical galaxy and at the Eastern edge of our I band image there is a merging system consisting of two extended objects, one of which is quite elongated and exhibits tidal arms. This object coincides with source #18.

4. Analysis

4.1. The source counts

In Table 3, we present the number of sources found in the FORS field and the source densities per square degree with fluxes $> 1, 1.5$ and 3×10^{-15} erg cm $^{-2}$ s $^{-1}$ in the soft band and the total number in the hard band. We find respectively 16, 12, 8 and 4 sources. It is instructive to compare our results with those of other deep *Chandra* observations. Therefore, we also report the densities found in two recent *Chandra* Deep Fields (Mushotzky et al. 2000; Giacconi et al. 2001), and the number of sources expected in the FORS field from these statistics. The table shows that the field of MRC 1138-262 contains about 50% more sources than the CDF in each of the three flux bins in the soft band (with a significance of about 1.5σ in each flux bin).

There are large field-to-field variations observed in surveys of the resolved components of the X-ray background, due to fluctuations of the large scale structure (the “cos-

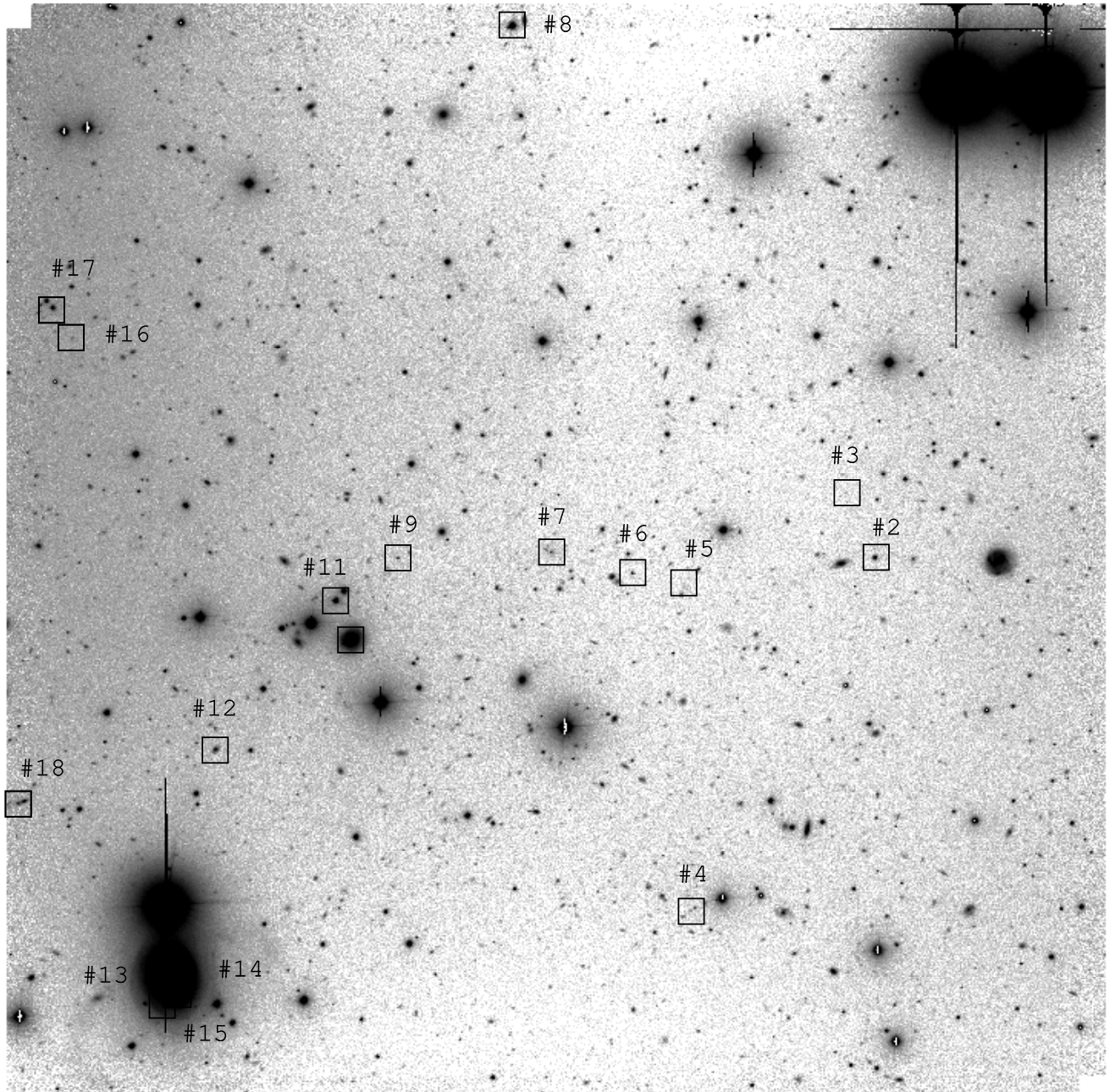


Figure 1 An I band image of the FORS field (approximately $6.8' \times 6.8'$) around the radio galaxy MRC 1138-262. The X-ray sources with optical identifications are indicated by squares and labelled as in Table 1. Source #7 is the radio galaxy. Sources #13 and #15 are within the spiral arms of galaxy #14.

mic variance”). Although the excess in the field of MRC 1138-262 is only 50%, this is still larger than the 20–30% observed amplitude of the cosmic variance (e.g. Cappi et al. 2001). Moreover, no comparable excess is observed in the hard band, although the statistics are poorer: the density of the four detected objects with flux $> 10^{-14}$ erg $\text{cm}^{-2} \text{s}^{-1}$ is ~ 250 sources deg^{-2} , consistent with the CDF results of 200–300 sources deg^{-2} .

We conclude that we have found a true over-density of soft X-ray sources in the field around MRC 1138-262. The density is similar to that revealed by Cappi et al. (2001) in two clusters of galaxies at $z \sim 0.5$: 3C295 and RXJ0030. They also find this surplus only in the soft band and not in

the hard band. Their most likely explanation of the over-density is that the clusters are atypical and contain more AGN than other distant clusters. No other similar studies have been reported on the highest redshift known clusters ($z \sim 1$ –1.2) which have been observed with *Chandra*. We will discuss this further in the last section.

4.2. Properties of the serendipitous sources

Clues on the nature of the field X-ray sources come from their hardness ratios, optical morphologies and optical to X-ray spectral indices.

Table 3. X-ray point source counts

Flux	Total	Exp CDF	n(1138)	n(CDF)
(1)	(2)	(3)	(4)	(5)
Soft band (0.5–2 keV)				
1.0	16	10.3/11	1040±260	670/720
1.5	12	7.2/8.3	780±220	470/540
3.0	8	4.0/5.1	520±180	260/330
Hard band (2–10 keV)				
10	4	3.7/5.4 ^a	260±130	240/350 ^a

Notes: (1) Minimum source flux in 10^{-15} erg cm^{-2} s^{-1} (2) Number of X-ray sources detected in the FORS field of MRC 1138-262 (3) Number of X-ray sources expected in a FORS-sized field from *Chandra* Deep Field counts; the two values are from the South and North surveys respectively (Giacconi et al. 2001, Mushotzsky et al. 2000) (4) Density with Poisson error (deg^{-2}) of X-ray sources in the field of MRC 1138-262 (5) Density (deg^{-2}) of X-ray sources from the two *Chandra* Deep Field surveys

^a the CDF North result was derived using $\Gamma = 1.4$ and not $\Gamma = 1.7$.

Due to the paucity of photons in individual sources, their spectral properties can best be studied by the hardness ratio (HR). The distribution of the hardness ratios as a function of the soft band flux is shown in the lower panel of Fig. 2. The HR of the sources indicate that most are soft, as expected from objects initially detected in the soft band, with the exception of source #18. The average value of the HR is -0.51, similar to that observed for type I AGN with a broad range of redshifts (e.g. Tozzi et al. 2001). The hardness ratio does not appear to depend on the soft X-ray flux, consistent with Tozzi et al. (2001), who show that the number of hard sources increases only at fluxes lower than our limit of 10^{-15} erg s^{-1} cm^{-2} . The only hard source in the sample is #18: as noted in Sect. 3 it coincides with the faintest of a pair of interacting objects. Its HR is consistent with a type II AGN at intermediate redshift ($z \sim 1$) with intrinsic absorbing column of the order of $N_{\text{H}} \sim 10^{23}$ cm^{-2} (assuming that it has an average spectrum with $\Gamma = 1.7$).

How do the optical counterparts of the X-ray sources compare with those found in the literature? We find that approximately one third of the sources are extended and two thirds of the sources appear pointlike. These numbers are similar to those found by Giacconi et al. (2001). Note that the resolution of the images is about 0'.6–0'.7, which at redshift 2 corresponds to 5–6 kpc, i.e. not a very stringent limit. Even starburst galaxies at moderately high redshift are expected to be unresolved at this resolution.

In the upper panel of Fig. 2, we plot the X-ray to R band flux ratio as a function of X-ray soft band flux: the values are in general consistent with those found by Lehmann et al. (2001) in the *ROSAT* Deep Survey, for sources with a similar range of soft band fluxes. They found that most of the AGN population (both broad line and narrow line AGN) cluster around a best fit line $S_x/S_o = 1$ (or $\log(S_x/S_o) = 0$). Similarly Stocke et al.

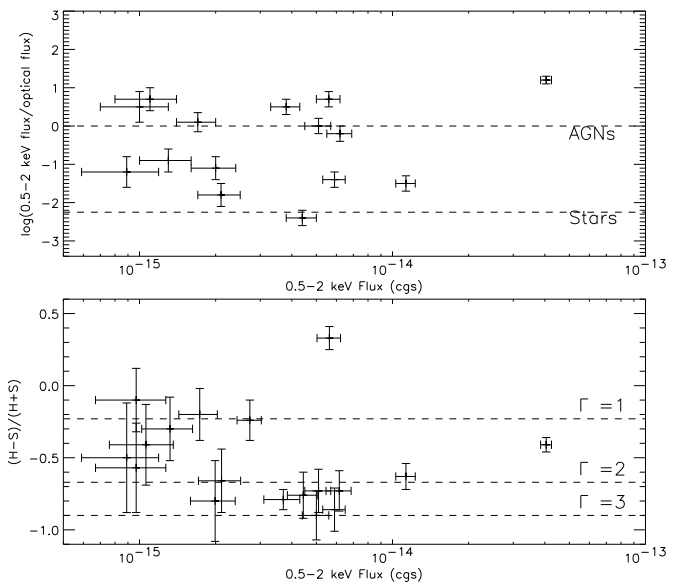


Figure 2 Upper panel: the soft X-ray to optical flux ratio versus the soft X-ray flux. The dotted lines give the typical ratios for AGN (upper) and stars (lower) as determined by Stocke et al. (1991). Lower panel: the hardness ratio $(H-S)/(H+S)$ versus the soft band flux for all sources. The dashed lines show power law models with different photon indices (Γ) computed assuming the galactic value $N_{\text{H}} = 4.5 \times 10^{20}$ cm^{-2} .

(1991) find that AGN all have a logarithmic ratio > -1 , whereas objects with a logarithmic ratio < -2 are probably galactic stars. Our plot indicates that most of the objects have properties consistent with AGN, while object #8 is most probably a star.

Tozzi et al. (2001) find a population of soft ($\text{HR} \sim -1$), low luminosity sources with low X-ray to optical ratio and X-ray soft band flux $< 3 \times 10^{-15}$ erg s^{-1} cm^{-2} which appear to be galaxies (as opposed to AGN) and are located at low or intermediate redshifts with an average $\bar{z} \sim 0.2$ –0.3. Their X-ray emission is probably produced by low power nuclear activity. In our sample, three sources (#2, #10 and #17) have low enough fluxes (they are detected only in the soft band) and X-ray to optical flux ratio ($\log(S_x/S_o) \leq -1$) to satisfy the above criteria (see upper panel of Fig. 2). Source #10 is indeed identified with a low redshift spiral galaxy, whereas the other two are unresolved so they could be small intermediate redshift galaxies hosting low power AGN.

5. Discussion

As noted in Sect. 4.1, there is an excess of soft X-ray sources as compared to deep field counts. The origin of this excess can be explained by the number of X-ray sources which are or could be associated with the $z \sim 2.16$ proto-cluster around the radio galaxy MRC 1138-262 (Pentericci et al. 2000).

Indeed the redshifts of two of the X-ray emitters (#3 and #6) have been confirmed spectroscopically. For two more (#9 and #16), there is a very good indication of

their redshift from the presence of excess flux in the optical narrow band corresponding to Ly α emission at the redshift of the radio galaxy. Source #5, the ERO, has colours consistent with a redshift ~ 2 object, so it could also be part of the protocluster. Finally, it is possible that other objects, in particular the optically fainter sources such as #4, are also located in the protocluster. Plausibly then, 5 or 6 sources are part of the protocluster at $z = 2.16$. Subtracting this number from the total detected sources in the field of MRC 1138-262, the number of remaining sources are fully consistent with the Deep Field measurements in all flux bins. None of the sources at $z \sim 2.16$ are detected in the hard X-ray band, so the statistics for this band also remain consistent with the Deep Field results.

For the remainder of this discussion, we will assume that these sources are indeed all at redshift ~ 2.16 . What powers the X-ray emission in the sources associated with the cluster? Are they AGN or powerful starburst galaxies? Based on the X-ray and optical properties discussed in the previous section, we conclude that they are most probably all AGN. Furthermore, the implied X-ray luminosities are far too large to be due to starbursts. The optical and NIR spectra of the two sources with known redshift, showing very broad emission lines (with widths of several 1000 km s^{-1}), also confirm that they are AGN.

Is it unusual to have such a high concentration of AGN at redshift ~ 2 ? We know that the density of AGN is a strong function of cosmic epoch: at $z = 2$ they were a hundred times more common than in the present universe (e.g. Boyle et al. 2000), so perhaps it is not surprising to find several of them in a $z = 2.16$ protocluster. From the soft X-ray luminosity function of AGN we can estimate how many sources we expect in a given region. At redshift ~ 2 the number of sources with luminosities $\log L_x$ between 43.6 and 45 is $6.4 \times 10^{-4} \text{ Mpc}^{-3}$ (according to Table 5 in Miyaji et al. 2001). For the 4758 Mpc^3 volume corresponding to the FWHM of the filter used for the detection of Ly α emitters (Kurk et al. 2000), three AGN would be expected. The protocluster around MRC 1138-262 contains about twice the number expected, which is quite unusual since normally clusters contain less AGN than the field. For example, in the nearby universe AGN occur rarely in clusters, comprising only 1% of all cluster galaxies (regardless of morphology, see Dressler et al. 1985), while they are much more common in the field population (about 5%, e.g. Huchra & Burg 1992). There is no evidence for an increase with redshift of the AGN fraction in clusters up to $z \sim 0.5$ (Dressler et al. 1999). We must point out, however, that most studies of this kind have been conducted with optical surveys where the dusty AGN or those with weak emission lines may not be recognized as such. Indeed, recent observations in other parts of the spectrum, including radio and X-rays, have shown unusual abundances of AGN in several clusters: Molnar et al. (2002) recently reported an excess number of X-ray sources around the cluster A1995 ($z=0.32$), and we already mentioned 3C295 at $z = 0.46$ and RX0030 at $z = 0.5$ (Cappi et al. 2001; Dressler and Gunn 1983).

In addition, Best et al. (2002) found a higher proportion of radio sources identified with AGN in the rich cluster MS1054-03 at $z = 0.83$ than in the field. Finally, *Chandra* observations of the cluster Abell 2104 at $z = 0.154$ reveal an unexpectedly high AGN fraction (Martini et al. 2002). Five out of six AGN in this cluster would not have been classified as such based on their optical spectra. In conclusion, we do not yet have proper statistics on the AGN fraction in clusters and on how this evolves up to the redshift of MRC 1138-262.

Finally, we draw attention to the string of X-ray emitters formed by the radio galaxy (#7) and sources #3, #5, #6 and #9, roughly along the East-West direction, as shown in Fig. 1. This string of X-ray sources, containing objects at redshifts close to that of the radio galaxy, is aligned with the axis of the radio emission of the central galaxy and with the general distribution of H α emitters in the cluster (see Kurk et al. 2002a). The extended X-ray emission associated with MRC 1138-262, which we interpreted as produced by gas shock heated by the expanding radio source, is also aligned along this axis (Carilli et al. 2002). All observations suggest that the ambient medium (gas and galaxies) is anisotropically distributed and that the radio jet has emerged along this direction, or is preferentially detected if it propagates along the direction of highest ambient density. As it seems, the ambient medium is distributed similarly both on small scales (100 kpc) and large scales (1–2 Mpc). West (1994) has extensively discussed a hierarchical formation scenario of massive cD galaxies being built up from smaller protogalactic units, resulting in a remarkable coherence of structures from the central engines of AGN to the large scale structure of the universe.

6. Conclusions

We have reported on the serendipitous X-ray emitters detected by *Chandra* in the field around the radio galaxy MRC 1138-262. We have presented optical identifications for 15 of the 18 sources from deep VLT observations. Based on the X-ray and optical properties of the sources, we conclude that most are type I AGN, one is a type II AGN and one is probably a star. Compared to the $\log N - \log S$ relation measured in deep *Chandra* observations, we find an excess of soft X-ray sources in the field of MRC 1138-262. The most probable explanation is that several of the X-ray emitters are associated with the $z \sim 2.16$ protocluster around the radio galaxy. Indeed, two of these have been confirmed spectroscopically to be broad emission line AGN at a redshift similar to that of the central galaxy. Additional spectroscopy is needed to determine how many of the X-ray emitters are really associated with the $z \sim 2.16$ protocluster. Furthermore, future observations of AGN in other distant cluster of galaxies will help to clarify whether the concentration of AGN around MRC 1138-262 is unusual or just typical for such a structure at high redshift.

Acknowledgements. The National Radio Astronomy Observatory (NRAO) is operated by Associated Universities, Inc. under a cooperative agreement with the National Science Foundation. CC and DH acknowledge support from grants from the Chandra X-ray Center. Work at SAO was partially supported by NASA grant GO0-1137B and contract NAS8-39073.

References

Bertin, E., & Arnouts, S. 1996, A&AS, 117, 393

Boyle, B. J., Shanks, T., Croom, S. M. et al. 2000, MNRAS, 317, 1014

Carilli, C. L., Harris, D. E., Pentericci, L., et al. 2002, ApJ, 567, 781

Cappi, M., Mazzotta, P., Elvis, M. et al. 2001, ApJ, 548, 624

Dobrzański, A., Ebeling, H., Glotfelty, K. et al. 1999, CHANDRA Detect 1.0 User Guide (Cambridge: Chandra X-Ray Center)

Dressler, A., Smail, I., Poggianti, B. M. et al. 1999, ApJS, 122, 51

Dressler, A., Thompson, I. B., & Shectman, S. A. 1985, ApJ, 288, 481

Dressler, A., & Gunn, J. E. 1983, ApJ, 270, 7

Elston, R., Rieke, G. H., & Rieke, M. J. 1988, ApJL, 331, L77

Freeman, P. E., Kashyap, V., Rosner, R., & Lamb, D. Q. 2002, ApJS, 138, 185

Kurk, J. D., Röttgering H. J. A., Pentericci, L., et al. 2000, A&A, 358, L1

Kurk, J. D., et al. 2002a submitted

Kurk, J. D., et al. 2002b submitted

Giacconi, R., Rosati, P., Tozzi, P., et al. 2001, ApJ, 551, 624

Lehmann, I., Hasinger, G., Schmidt, M., et al. 2001, A&A, 371, 833

Miyaji, T., Hasinger, G., & Schmidt, M. 2001, A&A, 369, 49

Molnar, S. M., Hughes, J. P., Donahue, M., & Joy, M. 2002, ApJL, 573, L91

Monet, D. B. A., et al. 1998, in VizieR On-line Data Catalog, 1252

Moshir, M. et al. 1990, IRAS faint Source Catalog, Version 2.0

Mushotzky, R. F., Cowie, L. L., Barger, A. J., & Arnaud, K. A. 2000, Nature, 404, 459

Pentericci, L., Kurk J. D., Röttgering, H. J. A., et al. 2000, A&A , 361, L25

Pentericci, L., Röttgering, H. J. A., Miley, G. K. et al. 1997, A&A, 326, 580

Stark, A. A., Gammie, C. F., Wilson, R. W., et al. 1992, ApJS, 79, 77

Stocke, J. T., Morris, S. L., Gioia, I. M., et al. 1991, ApJS, 76, 813

Tozzi, P., Rosati, P., Nonino, M., et al. 2001, ApJ, 562, 42

West, M. J. 1994, MNRAS, 268, 79